The problem of reliable design of vector-field path following in the presence of uncertain course dynamics ?

by

Spandan Roy, Stefano Fari, Ximan Wang, Simone Baldi

Report No: IIIT/TR/2019/-1

Centre for Robotics
International Institute of Information Technology
Hyderabad - 500 032, INDIA
November 2019

The problem of reliable design of vector-field path following in the presence of uncertain course dynamics ⋆

Ximan Wang [**] **Spandan Roy** [**,****] **Stefano Farì** [***] **Simone Baldi** [*,**]

[*] *School of Mathematics, Southeast University, Nanjing, China*
[**] *Delft Center for Systems and Control, TU Delft, The Netherlands*
[***] *German Aerospace Center (DLR), Bremen, Germany*
[****] *Robotics Research Centre, International Institute of Information Technology Hyderabad, India (e-mails: {x.wang-15,s.baldi}@tudelft.nl, spandan.roy@iiit.ac.in, faristefano@gmail.com)*

Abstract: Reliable guidance of fixed-wing Unmanned Aerial Vehicles (UAVs) is challenging, as their high maneuverability exposes them to several dynamical changes and parametric uncertainties. Reliability of state-of-the-art guidance methods is often at stake, as these methods heavily rely on precise UAV course dynamics, assumed in a decoupled first-order form with known time constant. To improve reliability of guidance for fixed-wing UAVs, this work proposes a novel vector field law that can handle uncertain course time constant and state-dependent uncertainty in the course dynamics arising from coupling. Stability is studied in the Lyapunov framework, while reliability of the proposed method is tested on a software-in-the loop UAV simulator. The simulations show that, in the presence of such uncertainty, the proposed method outperforms the standard vector field approaches.

Keywords: Fixed-wing Unmanned Aerial Vehicles, guidance navigation and control, uncertain course dynamics, reliable design, software-in-the loop UAV simulator.

1. INTRODUCTION

Fixed-wing Unmanned Aerial Vehicles (UAVs) are emerging rapidly, as their simple structure ensures efficient aerodynamics that provide unprecedented autonomy, even when compared to rotary-wing UAVs (Wang et al. (2017)). However, fixed-wing UAVs are quite challenging to fly (i.e. to control): this is because their high maneuverability exposes them to several changes in the dynamics (depending on altitude, speed, weight, angle of attack, etc.) and several parametric uncertainties. In control of fixed-wing UAVs, one should distinguish at least two levels: the low-level or *attitude control*, and the high-level or *guidance/path follower* (Beard and McLain (2012)). At the low-level, most strategies rely on cascade proportional-integral-derivative (PID) controllers, sometimes enhanced with techniques such as gain scheduling (Poksawat et al. (2018)). Among the many strategies proposed for guidance (geometric (Invernizzi and Lovera (2018); Cho and Kim (2016); Invernizzi et al. (2019)), PID (Kim et al. (2014)), target circulation (Olavo et al. (2018)), acceleration-based (Galffy et al. (2019)), etc.), the *vector field* approach (Li and Horowitz (2001); Nelson et al. (2007) has become popular due to its intuitive combination of geometry and control (the method is based on the generation of a field of desired course inputs to be used by the attitude control): extensions of this idea have appeared in the sense of time-varying vector fields (Jiang et al. (2017)), tangent-plus-Lyapunov vector field for obstacle avoidance (Chen et al. (2013)), and vector field for formation control (Dimarogonas (2012); Oh et al. (2015)). Unfortunately, reliability of guidance methods is often put at stake by the need for precise knowledge of the wind and of the UAV course dynamics: first-order UAV course dynamics with known time constant are often assumed, and coupling effects among longitudinal and lateral motions are neglected (Beard and McLain (2012)). Since the literature has shown how the final performance of a guidance law severely degrades with uncertain UAV dynamics (Guo et al. (2017); Fari et al. (2019)), UAV adaptive control methods have been studied to attain reliability by adapting the control gains to uncertainties: the issue of unknown wind has been studied in (Zhou et al. (2017)); support vector regression for adaptive attitude control is studied in (Shin et al. (2011)); an adaptive control for automatic carrier landing (a special attitude problem) is proposed in (Zhen et al. (2019)).

Despite these studies, to the best of the authors' knowledge, no adaptive algorithm has been proposed in literature for the relevant problem of *reliable design of vector field guidance with no knowledge of UAV course dynamics and wind environment*. Such a problem is solved here for the first time. The main contribution of this work is achieving path following in spite of uncertain course time constant, state-dependent uncertainty (i.e. couplings) af-

⋆ This work was partly supported by the Fundamental Research Funds for the Central Universities grant no. 4007019109 (RECONSTRUCT), and by the special guiding funds "double first-class" grant no. 4007019201 (corresponding author: S. Baldi)

fecting the course dynamics, and uncertain wind. Stability is studied in the Lyapunov stability framework, and the effectiveness of the proposed method is tested on a realistic software-in-the loop UAV simulator that can simulate the UAV dynamics with the autopilot low-level layer. The simulations show that, in the presence of uncertainty, the proposed method is more reliable and outperforms standard vector field approaches. Note that in (Fari et al. (2019)) the same authors developed an adaptive VF that can adapt to uncertain wind, but not to uncertain time course time constant.

The rest of the paper is organized as follows: Sect. 2 describes which UAV guidance parameters are uncertain and why. Sects. 3 and 4 cover the standard and the proposed VF approaches. Simulations are in Sect. 5, with conclusions in Sect. 6.

2. UAV UNCERTAINTY SETTING

A fixed-wing UAV can be modelled using 6-DOF Euler-Lagrange equations of motions. However, for guidance and navigation purposes, the dynamics of the UAV are significantly simplified (cf. the procedures in Nelson et al. (2007); Jiang et al. (2017); Chen et al. (2013); Dimarogonas (2012); Oh et al. (2015)) under standard assumptions resulting in first-order UAV course dynamics

$$\dot{\chi} = \alpha(\chi_c - \chi) \tag{1}$$

where χ is the course of the UAV, an inertial-referenced angle representing the angle between the north and the ground velocity V_g; χ_c is the command course from the controller, and α is a *positive* constant that defines the response speed of the course-hold loop. Two comments with respect to (1) are in order:

1) The dynamics (1) *rely on the assumption that longitudinal and lateral dynamics are decoupled*: a more realistic course angle model is
$$\dot{\chi} = \alpha(\chi_c - \chi) + \Delta(\chi) \tag{2}$$
where $\Delta(\chi)$ is a state-dependent coupling disturbance, i.e. with possibly no a priori constant bound.
2) The steps in (Beard and McLain (2012)) show how α in (1) is *affected in a complex way by aerodynamic coefficients which cannot be perfectly known*, and can even change depending on the operating conditions (altitude, velocity, etc.). Therefore, the parameter α should be considered as uncertain.

The wind triangle of Fig. 1 shows how the wind field affecting the UAV airspeed V_a consists not only of a constant (possibly known) wind component with magnitude W and angle ψ_W, but also of unknown and time-varying wind perturbations with amplitude $A(t)$ and angle $\psi_A(t)$. That is, the wind introduces another source of uncertainty. Traditionally, the uncertainty coming from the time-varying wind is neglected, which results in the following navigational dynamics of the UAV:

$$\begin{aligned} \dot{x} &= V_a \cos\psi + W \cos\psi_W = V_g \cos\chi \\ \dot{y} &= V_a \sin\psi + W \sin\psi_W = V_g \sin\chi \end{aligned} \tag{3}$$

where ψ is the heading angle between airspeed and horizontal axis in earth frame, x and y are the coordinate of the earth frame. Another comment follows:

3) The uncertainty in (3) is reflected in the fact that *the actual ground speed is not known* since the time-varying wind influences V_g, as shown in Fig. 1.

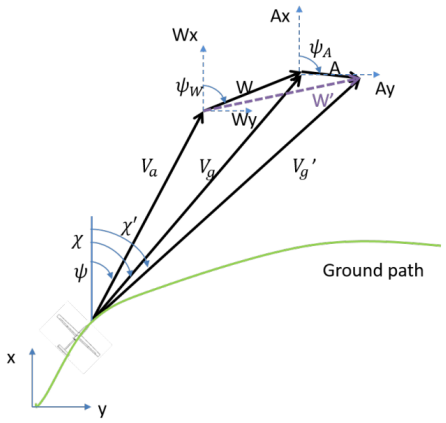

Fig. 1. The wind triangle for a fixed-wing UAV.

3. STANDARD VECTOR-FIELD PATH FOLLOWING

The problem is the one of guiding the UAV along some paths. In literature, two primitive paths are considered: the straight line and the orbit path. The vector field (VF) method is based on specifying a desired course at a certain coordinate.

3.1 Straight-Line Path Following

As in (Nelson et al. (2007)), let us consider for simplicity and without loss of generality a straight line parallel to the x-axis. The VF which describes the reference course to drive the UAV on the line is

$$\chi_d(e_y) = -\chi_\infty \frac{2}{\pi} \tan^{-1}(k e_y) \tag{4}$$

where e_y is the cross-track error (i.e. distance in the y-direction), χ_∞ is a parameter in $(0, \frac{\pi}{2}]$ which is the course reference when the error is large, and k a tuning parameter governing the VF smoothness. If the straight line is not parallel to y, it suffices to use the rotation matrix from the inertial frame to the path frame. In (Nelson et al. (2007)) it is shown that the control law which is able to let $\chi \to \chi_d$ and $e_y \to 0$ as $t \to \infty$ is

$$\chi_c = \chi - \chi_\infty \frac{2}{\pi} \frac{\beta_s V_g}{\alpha} \sin(\chi - \chi_q) - \frac{\kappa}{\alpha} \text{sat}\left(\frac{\tilde{\chi}}{\varepsilon}\right) \tag{5}$$

where $\tilde{\chi} = \chi - \chi_d$, $\beta_s = k/(1+(k e_y)^2)$, κ and ε are parameters governing control aggressiveness and counteracting a possible chattering in the control action, and

$$\text{sat}(x) = \begin{cases} x & \text{if } |x| < 1, \\ \text{sgn}(x) & \text{otherwise.} \end{cases} \tag{6}$$

3.2 Orbit Path Following

The strategy for orbit path following is similar to the straight line following, i.e. a desired course VF is built up around the desired orbit:

$$\chi_d(\tilde{d}) = \gamma + \lambda\left(\frac{\pi}{2} + \tan^{-1}(k\tilde{d})\right) \tag{7}$$

where is $\tilde{d} = d - R$, d is the distance of the UAV from the orbit center, R the orbit radius and γ is the angle

between the north and the UAV position with respect to the orbit center. For easiness of analysis, the UAV position is expressed in the circular coordinates where the origin locates at the orbit center. The parameter λ is 1 for clockwise orbit path and -1 for counter-clockwise orbit path. In (Nelson et al. (2007)) it is shown that the control law which is able to let $\chi \to \chi_d$ and $\tilde{d} \to 0$ as $t \to \infty$ is

$$\chi_c = \chi + \frac{V_g}{\alpha d}\sin(\chi-\gamma) + \beta\frac{\lambda V_g}{\alpha}\cos(\chi-\gamma) - \frac{\kappa}{\alpha}\,\mathrm{sat}\left(\frac{\tilde{\chi}}{\varepsilon}\right) \quad (8)$$

where $\beta = k/(1+(k\tilde{d})^2)$, and the parameters k, κ, ε are defined similarly to the straight-line case. The proof of the Lyapunov stability for (5) and (8) is given in (Nelson et al. (2007)) and will not be further discussed. Some remarks on (5) and (8) follow.

Remark 1. The guidance laws (5) *and* (8) *require precise knowledge of the course dynamics and of the wind, i.e. they require precise knowledge of* α *and* V_g *in* (1) *and* (3)*. Furthermore, the standard VF relies on the absence of perturbation in the course dynamics, i.e.* (1)*. For such ideal dynamics asymptotic tracking is concluded, or even finite-time tracking when the saturation function* (6) *is replaced by the sign function. However, such results cannot be obtained when* (1) *are replaced by* (2)*.*

In view of the above considerations, we will introduce a state-dependent perturbation in the course dynamics and uncertainty in α and V_g.

3.3 Uncertainty setting

The following state dependency of Δ is assumed:

$$|\Delta(\chi)| \le \kappa_0 + \kappa_1 |\tilde{\chi}| \quad (9)$$

for some unknown positive constants κ_0, κ_1. Notice that (9) is a quite general condition, as it includes the fact that $\Delta(\chi)$ *may not be bounded a priori.*

Instead of assuming exact knowledge of α, let us consider a nominal course time constant, named $\hat{\alpha}$, and satisfying

$$\left|\frac{\alpha}{\hat{\alpha}} - 1\right| = E < 1 \quad (10)$$

for some design parameter E. It can be noticed that the uncertainty set (10) requires $\hat{\alpha}$ to be not far from the actual α, i.e. $\alpha < (1+E)\hat{\alpha}$.

4. ADAPTIVE VECTOR-FIELD PATH FOLLOWING

In the presence of wind and course uncertainty, we introduce estimators for the wind vector V_g and for the course parameter α: we refer to the approach as *adaptive VF path following.*

4.1 Straight-Line Path Following

The following new adaptive guidance law is proposed

$$\chi^c = \underbrace{-\frac{\Lambda}{\hat{\alpha}}\tilde{\chi} + \chi}_{\text{LINEAR ACTION}} \underbrace{-\frac{1}{\hat{\alpha}}\chi^\infty \frac{2}{\pi}\frac{k}{1+(ke_y)^2}\hat{V}_g\sin(\chi)}_{\text{NOMINAL ACTION}} \underbrace{-\hat{\bar{\alpha}}\chi^\infty\frac{2}{\pi}\frac{k}{1+(ke_y)^2}\hat{V}_g\sin(\chi)}_{\text{COMPENSATION}} \underbrace{-\frac{\hat{\kappa}_0+\hat{\kappa}_1|\tilde{\chi}|}{\hat{\alpha}(1-E)}\,\mathrm{sat}(\frac{\tilde{\chi}}{\varepsilon})}_{\text{ROBUST ACTION}} \quad (11)$$

where $\hat{\kappa}_0$ and $\hat{\kappa}_1$ represent the estimated of κ_0 and κ_1 in (9), and Λ is a user-defined parameter that should satisfy $\Lambda > \frac{\kappa_0}{\varepsilon(1-E)}$. A short explanation for the different components is given in (11). The control law (11) is augmented with the following adaptive laws:

$$\begin{aligned}
\dot{\hat{V}}_g &= \Gamma_V \rho\tilde{\chi}\chi^\infty\frac{2}{\pi}\frac{k}{1+(ke_y)^2}\sin(\chi)\\
\dot{\hat{\bar{\alpha}}} &= \Gamma_\alpha\rho\tilde{\chi}\chi^\infty\frac{2}{\pi}\frac{k}{1+(ke_y)^2}\hat{V}_g\sin(\chi)\\
\dot{\hat{\kappa}}_0 &= \Gamma_0\rho|\tilde{\chi}|, \qquad \dot{\hat{\kappa}}_1 = \Gamma_1\rho|\tilde{\chi}|^2
\end{aligned} \quad (12)$$

with Γ_V, Γ_α, Γ_0, Γ_1 being user-defined gains. A stability proof for the proposed approach is given in the appendix.

4.2 Orbit Path Following

For the orbit, the standard guidance law is modified according to a similar philosophy as the straight line

$$\begin{aligned}
\chi^c = \quad & \underbrace{-\frac{\Lambda}{\hat{\alpha}}\tilde{\chi} + \chi}_{\text{LINEAR ACTION}} \quad \underbrace{-\frac{\hat{\kappa}_0+\hat{\kappa}_1|\tilde{\chi}|}{\hat{\alpha}(1-E)}\,\mathrm{sat}\left(\frac{\tilde{\chi}}{\varepsilon}\right)}_{\text{ROBUST ACTION}}\\
& \underbrace{-\hat{\bar{\alpha}}\hat{V}_g\left(\frac{\sin(\chi-\gamma)}{d} - \frac{k}{1+(k\tilde{d})^2}\cos(\chi-\gamma)\right)}_{\text{COMPENSATION}}\\
& \underbrace{-\frac{1}{\hat{\alpha}}\hat{V}_g\left(\frac{\sin(\chi-\gamma)}{d} - \frac{k}{1+(k\tilde{d})^2}\cos(\chi-\gamma)\right)}_{\text{NOMINAL ACTION}}
\end{aligned} \quad (13)$$

together with the adaptive laws

$$\begin{aligned}
\dot{\hat{V}}_g &= \Gamma_V\rho\tilde{\chi}\left(\frac{\sin(\chi-\gamma)}{d} - \frac{k}{1+(k\tilde{d})^2}\cos(\chi-\gamma)\right)\\
\dot{\hat{\bar{\alpha}}} &= \Gamma_\alpha\rho_2\tilde{\chi}\left(\frac{\sin(\chi-\gamma)}{d} - \frac{k}{1+(k\tilde{d})^2}\cos(\chi-\gamma)\right)\hat{V}_g\\
\dot{\hat{\kappa}}_0 &= \Gamma_0\rho|\tilde{\chi}|, \qquad \dot{\hat{\kappa}}_1 = \Gamma_1\rho|\tilde{\chi}|^2
\end{aligned} \quad (14)$$

with similar constants as the straight line case. A stability proof follows similar lines as the straight-line case.

Remark 2. As compared to standard VF (Nelson et al. (2007); Jiang et al. (2017); Chen et al. (2013); Dimarogonas (2012); Oh et al. (2015)), estimators for the ground velocity V_g *and for the course time constant* α *are incorporated in the control law, which are the first two estimators in* (12) *and* (14)*: in addition, two other gains are estimated via the last two in* (12) *and* (14) *which form an estimate of the state-dependent uncertainty (note that* $\hat{\kappa}_0 + \hat{\kappa}_1|\tilde{\chi}|$ *in* (11) *and* (13) *replaces the a priori bounded uncertainty* κ *in the standard VF* (5) *and* (8)*). In fact, a priori bounded uncertainty is restrictive (Obeid et al. (2018)) and should be avoided for practical systems (Roy et al. (2019)).*

Remark 3. It is evident from the wind triangle of Fig. 1 that V_g *is course-dependent because of the vector summation between* V_a *and* W*. To take into account course dependency of* V_g *(neglected by the standard VF method), the ground velocity estimator can be modified as*

$$\dot{\hat{V}}_g = \Gamma_V\rho\tilde{\chi}\left(\frac{\sin(\chi-\gamma)}{d} - \frac{k}{1+(k\tilde{d})^2}\cos(\chi-\gamma)\right) + F_o \quad (15)$$

where F_o is a feedforward term calculated as

$$F_o = \frac{\partial \hat{V}_g}{\partial \chi}\left[\frac{\hat{V}_g}{d}\sin(\chi-\gamma) + \lambda\beta_o\hat{V}_g\cos(\chi-\gamma) - \kappa\,\mathrm{sat}\left(\frac{\tilde{\chi}}{\epsilon}\right)\right]$$

and $\partial\hat{V}_g/\partial\chi$ calculated from the wind triangle as in (Zhou et al. (2017)). A similar idea applies to the straight line.

Remark 4. It is discussed in (Nelson et al. (2007)) that the standard VF is a sliding mode controller. By looking at the last two adaptation laws in (12) *and* (14) *it can be noticed that $\hat{\kappa}_0$ and $\hat{\kappa}_1$ monotonically increase according to the error, a celebrated adaptive strategy in the sliding mode community where a constant κ is replaced by a monotonically increasing one (Plestan et al. (2010)). Therefore, the proposed adaptive VF sits in the adaptive sliding mode framework: to avoid monotonic increase, suitable modifications proposed in literature (leakage or boundary layer adaptation (Roy and Baldi (2019))) can be used here as well, and are not shown due to space limitations.*

5. SIMULATION RESULTS

In this section, the performance of the proposed adaptive VF is assessed, as compared to the standard VF and to an ideal VF method, with the following wind knowledge:

- Standard VF (Nelson et al. (2007)): only the constant wind component is assumed to be known;
- Ideal VF (Fari et al. (2019)): both constant and time-varying wind components are assumed to be known;
- Adaptive VF (proposed): all wind components are estimated.

5.1 Software-in-the-loop UAV platform

With the purpose of testing the algorithms in a realistic UAV simulation platform, a software-in-the-loop UAV platform that can replicate the low-level control structure of the UAV (i.e. autopilot layer) was developed at TU Delft. More details on the software-in-the-loop UAV platform can be found in (Yang et al. (2019)).

In the numerical studies done in this work, we take the following environmental conditions: the constant wind amplitude is $W = 6$ with wind angle $\psi_W = 230°$; a time-varying wind is considered whose magnitude changes over time in a cosinusoidal fashion with frequency 0.1 rad/sec and whose angle changes in a sinusoidal fashion with frequency 0.1 rad/sec. In addition, Dryden turbulence was considered. All these environmental conditions have been combined together to obtain four different wind scenarios, summarized in Table 1.

Table 1. Flight environmental conditions

Scenario	Constant wind	Turbulence	Time-var. wind
#1	No	No	No
#2	Yes	No	No
#3	Yes	Yes	No
#4	Yes	Yes	Yes

The standard and the ideal VF assume $\alpha = 0.42$ in (5) and (8). However, the exact knowledge of α is not available, because the software-in-the-loop UAV dynamics are much more complex than (1). As compared to the standard (and ideal) VF, the proposed adaptive VF uses a nominal $\hat{\alpha} = 0.42$, and is the only approach that tries to compensate for such lack of knowledge.

5.2 Comparisons

The performance of the standard, adaptive and ideal VF are evaluated using the RMS steady-state error. The parameters in straight line and orbit path controller, summarized in Table 2, have been tuned so as to find a good compromise between convergence speed and no oscillations. As in the original VF paper (Nelson et al. (2007)), the scaling parameter ρ is chosen as $(e_y(0)/\pi)^2$ and $(\tilde{d}(0)/\pi)^2$, for straight line and orbit respectively. For the adaptive VF to start in similar conditions as the standard VF we initialize $\hat{\kappa}_0(0) = \kappa$, $\hat{\kappa}_1(0) = 10^{-5}$ and $\hat{\tilde{\alpha}}(0) = 0$ (initial estimates of uncertainty in Δ and α).

Tables 3 and 4 highlight how the proposed adaptive VF outperforms, in all scenarios, even the ideal VF: this is due to the fact that the knowledge of $\alpha = 0.42$ is not accurate. Remarkably, the adaptive VF is the only one in Scenario #1 that is able to perfectly track the orbit, whereas the other approaches cannot, due to the unmodelled dynamics. This can be clearly seen in Fig. 2. The reason for such improved performance is that the proposed adaptive VF is able to 'automatically tune' the control parameters $\hat{V}_g$ and $\hat{\tilde{\alpha}}$ in such a way to reduce the error, as it can be seen in Fig. 3.

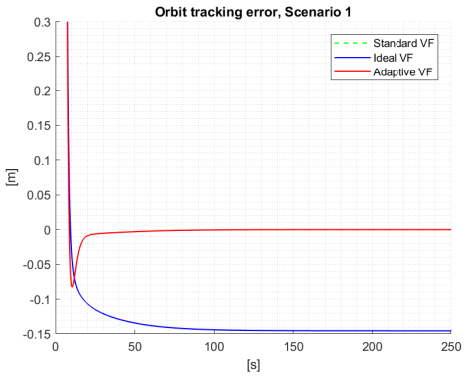

Fig. 2. Orbit tracking error under Scenario 1 (the ideal VF coincides with the standard VF)

In Scenario #2, the proposed adaptive VF reduces the oscillations of the error (present due to the course dependent effect of the wind), cf. Fig. 4. A similar reasoning applies to Scenarios #3 and #4, which are not shown for lack of space. As compared to the standard VF, the improvements are above 11% for the straight line in all scenarios, and

Table 2. The parameter values of the adaptive control law

	ρ	Γ_V	Γ_0, Γ_1	Γ_α
Line	253.56	0.5	10^{-5}	0.5
Orbit	1584.75	0.5	10^{-5}	0.5

	χ^∞	k	ϵ
Line	$\pi/2$	0.1 m^{-1}	1 rad
Orbit	$\pi/2$	0.1 m^{-1}	1 rad

Table 3. Line path comparisons. Error reduction of adaptive VF vs. standard VF is noted.

Scenario	Standard VF	Ideal VF	Adaptive VF
#1	0	0	0
#2	0.6535	0.6528	0.5835 *(-11%)*
#3	0.6726	0.6726	0.5998 *(-11%)*
#4	1.2931	0.4750	0.4261 *(-67%)*

Table 4. Orbit path comparisons. Error reduction of adaptive VF vs. standard VF is noted.

Scenario	Standard VF	Ideal VF	Adaptive VF
#1	0.1456	0.1456	0 *(-100%)*
#2	0.7755	0.7755	0.4169 *(-46%)*
#3	0.8205	0.7976	0.4269 *(-48%)*
#4	0.5679	0.5471	0.2906 *(-49%)*

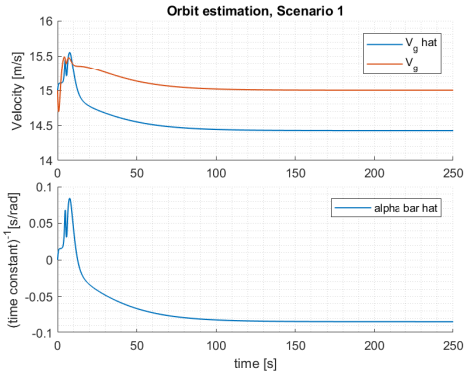

Fig. 3. Orbit estimation under Scenario 1

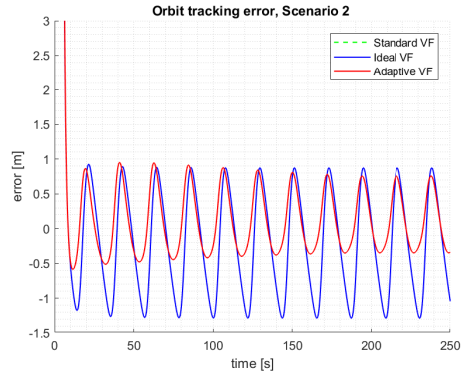

Fig. 4. Orbit tracking error under Scenario 2 (the ideal VF coincides with the standard VF)

above 46% for the orbit in all scenarios. With respect to the ideal VF, the improvements are above 7% for the straight line, and above 46% for the orbit.

6. CONCLUSIONS

AThis work has proposed a novel guidance law that does not require precise knowledge of the course time constant, while the course dynamics can be affected by state-dependent uncertainty representing couplings. The effectiveness of the proposed method in handling such uncertainty was tested on a software-in-the-loop UAV simulator. Persistency of excitation is important in uncertainty estimation: as recent works have appeared on adaptive control with reduced persistency of excitation (Cho et al. (2018); Roy et al. (2018)), an interesting future work is to study if/how such methods apply to UAVs.

REFERENCES

Beard, R.W. and McLain, T.W. (2012). *Small Unmanned Aircraft: Theory and Practice*.

Chen, H., Chang, K., and Agate, C.S. (2013). Uav path planning with tangent-plus-lyapunov vector field guidance and obstacle avoidance. *IEEE Transactions on Aerospace and Electronic Systems*, 49(2), 840–856.

Cho, N. and Kim, Y. (2016). Optimality of augmented ideal proportional navigation for maneuvering target interception. *IEEE Transactions on Aerospace and Electronic Systems*, 52(2), 948–954.

Cho, N., Shin, H., Kim, Y., and Tsourdos, A. (2018). Composite model reference adaptive control with parameter convergence under finite excitation. *IEEE Transactions on Automatic Control*, 63(3), 811–818.

Dimarogonas, D.V. (2012). Sufficient conditions for decentralized potential functions based controllers using canonical vector fields. *IEEE Transactions on Automatic Control*, 57(10), 2621–2626.

Fari, S., Wang, X., Roy, S., and Baldi, S. (2019). Addressing unmodelled path-following dynamics via adaptive vector field: a uav test case. *IEEE Transactions on Aerospace and Electronic Systems*. doi: 10.1109/TAES.2019.2925487.

Galffy, A., Böck, M., and Kugi, A. (2019). Nonlinear 3d path following control of a fixed-wing aircraft based on acceleration control. *Control Engineering Practice*, 86, 56 – 69.

Guo, Z., Zhou, J., Guo, J., Cieslak, J., and Chang, J. (2017). Coupling-characterization-based robust attitude control scheme for hypersonic vehicles. *IEEE Transactions on Industrial Electronics*, 64(8), 6350–6361.

Invernizzi, D., Lovera, M., and Zaccarian, L. (2019). Dynamic attitude planning for trajectory tracking in thrust-vectoring uavs. *IEEE Transactions on Automatic Control*. doi:10.1109/TAC.2019.2919660.

Invernizzi, D. and Lovera, M. (2018). Trajectory tracking control of thrust-vectoring uavs. *Automatica*, 95, 180 – 186.

Jiang, W., Wang, D., Wang, Y., and Ali, Z.A. (2017). Uav rendezvous based on time-varying vector fields. *Electronics Letters*, 53(10), 653–655.

Kim, J., Lee, D., Cho, K., Kim, J., and Han, D. (2014). Two-stage trajectory planning for stable image acquisition of a fixed wing uav. *IEEE Transactions on Aerospace and Electronic Systems*, 50(3), 2405–2415.

Li, P.Y. and Horowitz, R. (2001). Passive velocity field control (pvfc). part ii. application to contour following. *IEEE Transactions on Automatic Control*, 46(9), 1360–1371.

Nelson, D.R., Barber, D.B., McLain, T.W., and Beard, R.W. (2007). Vector field path following for miniature air vehicles. *IEEE Transactions on Robotics*, 23(3), 519–529.

Obeid, H., Fridman, L.M., Laghrouche, S., and Harmouche, M. (2018). Barrier function-based adaptive sliding mode control. *Automatica*, 93, 540–544.

Oh, H., Kim, S., Shin, H., and Tsourdos, A. (2015). Coordinated standoff tracking of moving target groups

using multiple uavs. *IEEE Transactions on Aerospace and Electronic Systems*, 51(2), 1501–1514.

Olavo, J.L.G., Thums, G.D., Jesus, T.A., de Araújo Pimenta, L.C., Torres, L.A.B., and Palhares, R.M. (2018). Robust guidance strategy for target circulation by controlled uav. *IEEE Transactions on Aerospace and Electronic Systems*, 54(3), 1415–1431.

Plestan, F., Shtessel, Y., Brégeault, V., and Poznyak, A. (2010). New methodologies for adaptive sliding mode control. *International Journal of Control*, 83(9), 1907–1919.

Poksawat, P., Wang, L., and Mohamed, A. (2018). Gain scheduled attitude control of fixed-wing uav with automatic controller tuning. *IEEE Transactions on Control Systems Technology*, 26(4), 1192–1203.

Roy, S., Basu Roy, S., Lee, J., and Baldi, S. (2019). Overcoming the underestimation and overestimation problems in adaptive sliding mode control. *IEEE/ASME Transactions on Mechatronics*, 1–1. doi: 10.1109/TMECH.2019.2930711.

Roy, S.B., Bhasin, S., and Kar, I.N. (2018). Combined mrac for unknown mimo lti systems with parameter convergence. *IEEE Transactions on Automatic Control*, 63(1), 283–290.

Roy, S. and Baldi, S. (2019). On reduced-complexity robust adaptive control of switched euler–lagrange systems. *Nonlinear Analysis: Hybrid Systems*, 34, 226–237.

Shin, J., Kim, H.J., and Kim, Y. (2011). Adaptive support vector regression for uav flight control. *Neural Networks*, 24(1), 109 – 120.

Wang, Y., Garcia, E., Casbeer, D., and Zhang, F. (2017). *Cooperative Control of Multi-Agent Systems: Theory and Applications*.

Yang, J., Wang, X., Baldi, S., Singh, S., and Fari, S. (2019). A software-in-the-loop implementation of adaptive formation control for fixed-wing uavs. *IEEE/CAA Journal of Automatica Sinica*, 6(5), 1230–1239.

Zhen, Z., Tao, G., Yu, C., and Xue, Y. (2019). A multivariable adaptive control scheme for automatic carrier landing of uav. *Aerospace Science and Technology*, 92, 714 – 721.

Zhou, B., Satyavada, H., and Baldi, S. (2017). Adaptive path following for unmanned aerial vehicles in time-varying unknown wind environments. In *2017 American Control Conference (ACC)*, 1127–1132.

Appendix A. STRAIGHT-LINE CASE: STABILITY

Consider the following Lyapunov function

$$W = \frac{1}{2}y^2 + \frac{1}{2}\rho\tilde{\chi}^2 + \frac{1}{2\Gamma_V}\tilde{V}_g + \frac{1}{2\Gamma_0}\tilde{\kappa}_0^2 + \frac{1}{2\Gamma_1}\tilde{\kappa}_1^2 + \frac{1}{2\Gamma_\alpha}\tilde{\bar{\alpha}}^2 \tag{A.1}$$

where $\tilde{V}_g = \hat{V}_g - V_g$, $\tilde{\kappa}_0 = \hat{\kappa}_0 - \kappa_0$, $\tilde{\kappa}_1 = \hat{\kappa}_1 - \kappa_1$, $\tilde{\bar{\alpha}} = \hat{\bar{\alpha}} - \bar{\alpha}$. The derivative for the Lyapunov function can be calculated

$$\begin{aligned}
\dot{W} &= y\dot{y} + \rho\tilde{\chi}\dot{\tilde{\chi}} + \frac{1}{\Gamma_V}\tilde{V}_g\dot{\tilde{V}}_g + \frac{1}{\Gamma_0}\tilde{\kappa}_0\dot{\tilde{\kappa}}_0 + \frac{1}{\Gamma_1}\tilde{\kappa}_1\dot{\tilde{\kappa}}_1 + \frac{1}{\Gamma_\alpha}\tilde{\bar{\alpha}}\dot{\tilde{\bar{\alpha}}} \\
&= yV_g\sin(\chi^d - \tilde{\chi}) + \rho\tilde{\chi}\left(\alpha(\chi^c - \chi) + \Delta\right. \\
&\left.+\chi^\infty\frac{2}{\pi}\frac{\kappa}{1+(\kappa y)^2}V_g\sin(\chi)\right) \\
&+ \frac{1}{\Gamma_V}\tilde{V}_g\dot{\hat{V}}_g + \frac{1}{\Gamma_0}\tilde{\kappa}_0\dot{\hat{\kappa}}_0 + \frac{1}{\Gamma_1}\tilde{\kappa}_1\dot{\hat{\kappa}}_1 + \frac{1}{\Gamma_\alpha}\tilde{\bar{\alpha}}\dot{\hat{\bar{\alpha}}}
\end{aligned} \tag{A.2}$$

$$\begin{aligned}
&= \underbrace{yV_g\sin(\chi^d - \tilde{\chi}) - \rho\frac{\tilde{\chi}^2}{\varepsilon}\kappa_0}_{\text{IDEAL}} + \rho\frac{\tilde{\chi}^2}{\varepsilon}\kappa_0 \\
&+ \rho\tilde{\chi}\left[\alpha(-\frac{\Lambda}{\hat{\alpha}}\tilde{\chi} + \chi - \frac{1}{\hat{\alpha}}\chi^\infty\frac{2}{\pi}\frac{\kappa}{1+(\kappa y)^2}V_g\sin(\chi)\right. \\
&-\frac{1}{\hat{\alpha}}\chi^\infty\frac{2}{\pi}\frac{\kappa}{1+(\kappa y)^2}\tilde{V}_g\sin(\chi) \\
&-\hat{\bar{\alpha}}\chi^\infty\frac{2}{\pi}\frac{\kappa}{1+(\kappa y)^2}\hat{V}_g\sin(\chi) - \chi) \\
&+\Delta + \frac{\alpha}{\hat{\alpha}}\chi^\infty\frac{2}{\pi}\frac{\kappa}{1+(\kappa y)^2}V_g\sin(\chi) \\
&+(1-\frac{\alpha}{\hat{\alpha}})\chi^\infty\frac{2}{\pi}\frac{\kappa}{1+(\kappa y)^2}\hat{V}_g\sin(\chi) \\
&\left.-\frac{\alpha}{\hat{\alpha}}\frac{\hat{\kappa}_0 + \hat{\kappa}_1|\xi|}{1-E}\,\mathrm{sat}(\frac{\tilde{\chi}}{\varepsilon}) - (1-\frac{\alpha}{\hat{\alpha}})\chi^\infty\frac{2}{\pi}\frac{\kappa}{1+(\kappa y)^2}\tilde{V}_g\sin(\chi)\right] \\
&+ \frac{1}{\Gamma_V}\tilde{V}_g\dot{\hat{V}}_g + \frac{1}{\Gamma_0}\tilde{\kappa}_0\dot{\hat{\kappa}}_0 + \frac{1}{\Gamma_1}\tilde{\kappa}_1\dot{\hat{\kappa}}_1 + \frac{1}{\Gamma_\alpha}\tilde{\bar{\alpha}}\dot{\hat{\bar{\alpha}}} \\
&= IDEAL + \rho\tilde{\chi}^2(\frac{\kappa_0}{\varepsilon} - \frac{\alpha}{\hat{\alpha}}\Lambda) \\
&+ \left[-\rho\tilde{\chi}\chi^\infty\frac{2}{\pi}\frac{\kappa}{1+(\kappa y)^2}\sin(\chi) + \frac{1}{\Gamma_V}\dot{\hat{V}}_g\right]\tilde{V}_g \\
&+ \left[-\rho\tilde{\chi}\alpha\chi^\infty\frac{2}{\pi}\frac{\kappa}{1+(\kappa y)^2}\hat{V}_g\sin(\chi) + \frac{1}{\Gamma_\alpha}\dot{\hat{\bar{\alpha}}}\right]\tilde{\bar{\alpha}} + \\
&\rho\tilde{\chi}\left[\Delta - \frac{\alpha}{\hat{\alpha}}\frac{\hat{\kappa}_0 + \hat{\kappa}_1|\xi|}{1-E}\,\mathrm{sat}(\frac{\tilde{\chi}}{\varepsilon})\right] \\
&+ \frac{1}{\Gamma_0}\tilde{\kappa}_0\dot{\hat{\kappa}}_0 + \frac{1}{\Gamma_1}\tilde{\kappa}_1\dot{\hat{\kappa}}_1
\end{aligned} \tag{A.3}$$

where $\bar{\alpha} = \frac{1}{\alpha}(1 - \frac{\alpha}{\hat{\alpha}}) = \frac{1}{\alpha} - \frac{1}{\hat{\alpha}}$ and the term $IDEAL$ has been used to represent the same term appearing in (Nelson et al. (2007)) due to the ideal course dynamics. To keep the analysis simple, we consider we are outside the saturation boundary of the saturation function (6), which amounts to replacing $\mathrm{sat}(\frac{\tilde{\chi}}{\varepsilon}) = \mathrm{sgn}(\frac{\tilde{\chi}}{\varepsilon})$. At this point we use the fact

$$\begin{aligned}
&\tilde{\chi}\frac{\alpha}{\hat{\alpha}}\frac{\hat{\kappa}_0 + \hat{\kappa}_1|\xi|}{1-E}\,\mathrm{sgn}(\frac{\tilde{\chi}}{\varepsilon}) \le -(1-E)\frac{\hat{\kappa}_0 + \hat{\kappa}_1|\xi|}{1-E}|\tilde{\chi}| \\
&\le -\hat{\kappa}_0|\tilde{\chi}| - \hat{\kappa}_1|\tilde{\chi}||\xi|
\end{aligned}$$

and finally obtain

$$\begin{aligned}
\dot{W} &\le IDEAL + \rho\tilde{\chi}^2(\frac{\kappa_0}{\varepsilon} - \frac{\alpha}{\hat{\alpha}}\Lambda) \\
&+ \left[-\rho\tilde{\chi}\chi^\infty\frac{2}{\pi}\frac{\kappa}{1+(\kappa y)^2}\sin(\chi) + \frac{1}{\Gamma_V}\dot{\hat{V}}_g\right]\tilde{V}_g \\
&+ \left[-\rho\tilde{\chi}\alpha\chi^\infty\frac{2}{\pi}\frac{\kappa}{1+(\kappa y)^2}\hat{V}_g\sin(\chi) + \frac{1}{\Gamma_\alpha}\dot{\hat{\bar{\alpha}}}\right]\tilde{\bar{\alpha}} \\
&+ \left[-\rho|\tilde{\chi}| + \frac{1}{\Gamma_0}\dot{\hat{\kappa}}_0\right]\tilde{\kappa}_0 + \left[-\rho|\tilde{\chi}||\xi| + \frac{1}{\Gamma_1}\dot{\hat{\kappa}}_1\right]\tilde{\kappa}_1
\end{aligned} \tag{A.4}$$

where the terms inside the square parentheses disappear thanks to the adaptive laws. The gain $\frac{\kappa_0}{\varepsilon} - \frac{\alpha}{\hat{\alpha}}\Lambda$ can be selected using:

$$\Rightarrow \frac{\kappa_0}{\varepsilon} - (1-E)\Lambda < 0, \text{ if} \Lambda > \frac{\kappa_0}{\varepsilon(1-E)} \tag{A.5}$$

This leads to $\dot{W} \le 0$ from which the same stability result in (Nelson et al. (2007)) can be obtained.